Journal of
Engineering Sciences
Faculty of Engineering
Assiut University
JES
مجلة
العلوم الهندسية
كلية الهندسة
جامعة أسيوط
journal homepage: http://jesaun.journals.ekb.eg

Vertical Accuracy Assessment of Digital Elevation Models Generated by Sentinel- 1A: A Case study: Eldabha, EGYPT

Received 5 April 2025; Revised 23 July 2025; Accepted 23 July 2025

Mohamed A. Besheer[1]
Doaa A. Mohammed[2]
Sonbaty A. Ahmed[3]
Farrag A. Farrag[4]

Keywords
Radar image , interferometry, DEM , sentinel-1A

Abstract: This research focuses on improving the vertical accuracy of Digital Elevation Models (DEMs) generated from Sentinel-1A satellite imagery. The study investigates the influence of Goldstein filtering, temporal baseline, and perpendicular baseline on DEM accuracy. Two DEMs were created for the Eldabha region using distinct baseline configurations: (a) a 24-day temporal baseline with a 160 m perpendicular baseline, and (b) a 12-day temporal baseline with a 230 m perpendicular baseline. Each DEM was generated both with and without the application of the Goldstein filter. Accuracy assessments were conducted using GNSS data, with evaluation metrics including Root Mean Square Error (RMSE), standard deviation (STD), mean error, and the range of elevation differences. The results indicate that model (b), which utilized the shorter temporal and larger perpendicular baselines along with Goldstein filtering, achieved the highest accuracy, yielding an RMSE of 12.00 meters. The findings underscore the importance of selecting suitable interferometric baselines and applying effective filtering techniques to enhance DEM quality.

1.Introduction

A wide variety of geospatial and environmental tasks rely heavily on Digital Elevation Models (DEMs), especially applications related to geography and environmental science. The growing accessibility of Synthetic Aperture Radar (SAR) datasets, particularly from Sentinel-1A, facilitates the generation of DEMs with enhanced spatial and temporal resolution[1]. Despite these advantages, SAR-derived DEMs often suffer from noise and decorrelation issues particularly prevalent in heterogeneous or complex terrain[2], [3]. To mitigate these effects and enhance vertical accuracy, filtering techniques such as the Goldstein filter are critical, as they improve coherence and contribute to the production of more reliable elevation models[4]. Launched in 2014, Sentinel-1A is a European radar satellite that is part of the EU's Copernicus initiative. It carries a C-band Synthetic Aperture Radar (SAR) and supports a wide array of applications, including the detection

[1] Civil engineering department , faculty of engineering, Assuit university, Assuit, Egypt (mabesheer@aun.edu.eg)
[2] Director of the spatial state administration, New Valley Governor, Egypt.(doaa.mohamed20@eng.aun.edu.eg)
[3] Civil Engineering department, faculty of engineering, Assuit university, Egypt (asonbaty@aun.edu.eg)
[4] Prof. of surveying and photogrammetry, Civil Eng. Dpt. Faculty of Engineering, Assiut University. (farrag@aun.edu.eg)

https://doi.org/10.21608/JESAUN.2025.372829.1470

of landslides, land subsidence, and flood mapping [5]. Due to its open data policy, Sentinel-1A has been extensively utilized for DEM generation in various geographic contexts. For instance, one study explored topographic mapping of the Greek islands Lesbos and Mykonos using Sentinel-1A data, comparing DEMs generated with small (175–350 m) and large (175–1,225 m) perpendicular baselines against ground control points. The average RMSE of the derived DSMs was approximately 19.48 m.[6].

Another study employed Sentinel-1A to create DEMs for the Cameron Highlands in Malaysia and Sanandaj in Iran, using a 14 m pixel resolution and ground control validation. The results showed that the accuracy was lower when compared to the SRTM, ALOS-PALSAR, TanDEM-X, and AIRSAR datasets. The reduced performance was attributed to C-band limitations in vegetated regions and insufficient perpendicular baselines, which were typically below 100 m[5]. For optimal DEM generation, the interferometric baseline is generally recommended to fall within the range of 150 to 300 meters to ensure a suitable balance between height sensitivity and coherence [7].

Supporting these findings,[8] assessed DEMs generated from various SAR datasets and reported that Sentinel-1A delivered reliable accuracy in flat regions but showed diminished performance in mountainous terrains when compared to datasets such as SRTM and ALOS PALSAR. Their study highlights that the accuracy of DEMs derived from Sentinel-1A is strongly influenced by terrain characteristics and acquisition parameters especially the geometry of the perpendicular baseline.

These findings underscore the need to investigate how interferometric parameters particularly baseline geometry and filtering methods influence DEM accuracy. The motivation for this research stems from the need to improve the precision of DEMs generated from Sentinel-1A SAR data. By investigating the effects of Goldstein filtering, temporal baselines, and perpendicular baselines on DEM accuracy, this study aims to optimize elevation modeling techniques. [9].

2.Methods and tools

Sentinel-1A imagery was acquired for two interferometric pairs. Model (a): 24-day temporal baseline, 160 m perpendicular baseline and model (b) with 12-day temporal baseline and 230 m perpendicular baseline. The data was processed using SNAP software, and DEMs were generated both with and without applying Goldstein filtering. To assess the vertical accuracy of the generated DEMs, a reference dataset was utilized based on high-accuracy Real-Time Kinematic (RTK) GNSS measurements. A total of [81005] RTK points were collected in February 2022 as part of a field survey for the “Egypt’s Future for Agricultural Production” sand dune protection project. The GNSS survey was conducted using dual-frequency receivers under open-sky conditions, achieving centimeter-level vertical accuracy. These RTK points provide orthometric heights, referenced to mean sea level through the EGM96 geoid model **.** Therefore, all DEMs were compared against this reference dataset in terms of orthometric height, ensuring consistency in the vertical reference system.These ground control points were used to generate a high-resolution reference DEM, which served as the benchmark for evaluating the vertical accuracy of the Sentinel-1A derived DEMs. Fig 1 shows the main steps for the methodology adobted to generate and evaluate DEM from Sentinel-1A imagery.

3. Pre-Processing

Study area located in the western desert, Egypt; between 29° 16′ 46.8152″ and 29° 21′ 58.9901″ longitude, 30° 18′ 13.7207″ and 30° 13′ 09.2888″ latitude as shown in Fig.2. Sentinel-1 satellite

carries a C-band Synthetic Aperture Radar (SAR) with wavelength 5.7 cm [10]. This research employs imagery exclusively acquired in the Interferometric Wide (IW) swath mode, which is optimized for interferometric applications such as Digital Elevation Model (DEM) generation. The IW mode utilizes the Terrain Observation with Progressive Scans (TOPS) technique, in which the radar antenna is periodically steered across three adjacent sub-swaths (IW1, IW2, and IW3) to cover a wide area. Suitable Sentinel-1A image pairs were selected using the Alaska Satellite Facility's online platform (https://asf.alaska.edu/), which provides tools for identifying image availability and baseline geometry. The specific acquisition parameters of the image pairs used in this study are presented in Table 1.

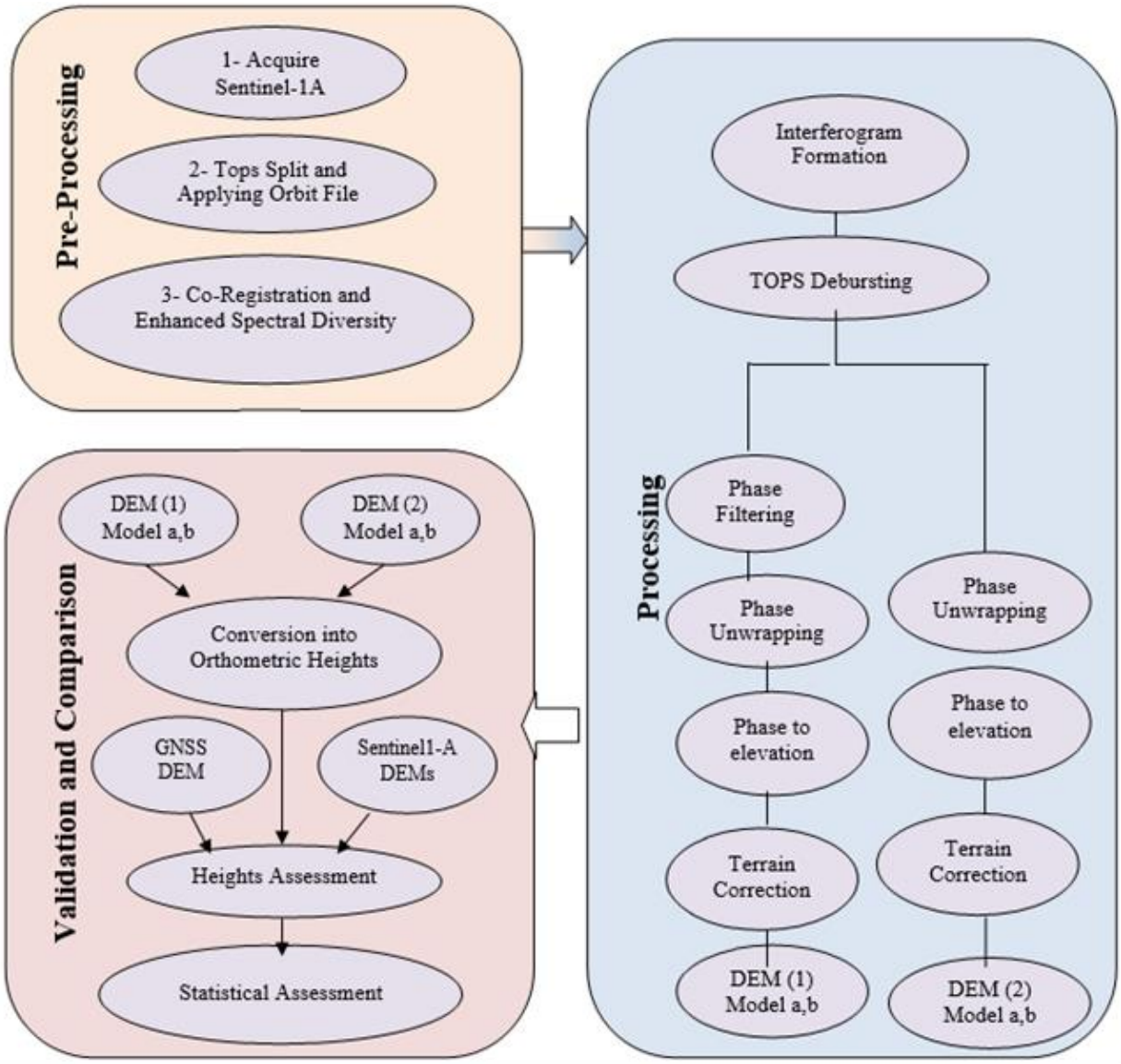

Fig.1: Main steps to generate and evaluate DEM

3.1. Tops Split and Applying Orbit File

The first step in the workflow is the co-registration of Imagery by applying orbit file information and Sentinel-1top split to the data to select only bursts which are required for the analysis [11]. For the area under consideration, burst number (5&6) and IW2 accord area of interest as shown Fig.2-b.

3.2. Co-Registration and Enhanced Spectral Diversity

Coregistration of Sentinel-1 imagery is an important step in the analysis of synthetic aperture

radar (SAR) images to guarantees that each ground target maintains the same range and azimuth. This process main purpous is to aligning different SAR images from different acquisition times to the same coordinate system, acquisitions must be stacked first. This is a crucial step in forming an interferogram [12]. Co-register the two split products based on the orbit information and information from Shuttle Radar Topography Mission (SRTM) 1arc sec DEM which is downloaded by SNAP program was used with bilinear interpolation resampling method. Back-geocoding (co-registration) tool in SNAP software was applied to align the two split satellite data based on the orbital information. In order to extract the phase difference to increase the quality of the co-registration process, Enhanced Spectral Diversity (ESD) [13] was applied on the stack generated by the Back Geocoding.

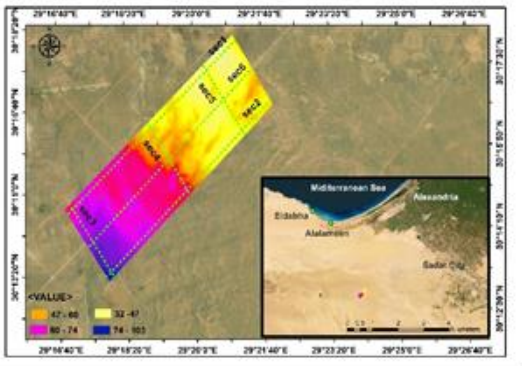

Fig. 2-a: Study area geographic location.

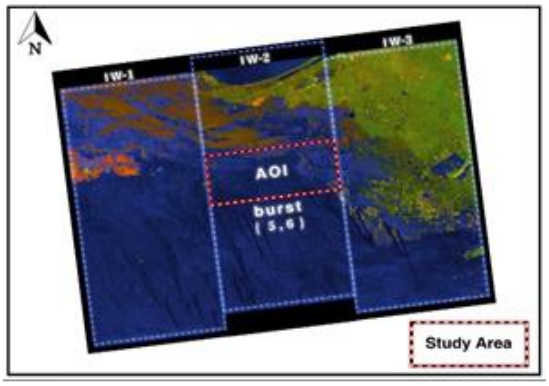

Fig. 2-b: Study area swath and burst location.

Fig .2: Study Area

Table 1: Features of the Sentinel-1A pair of images used in this study.

Pair image	Satellite	Mode	Reference /Secondary	Btemp /day	Pperp /m	Acquisition date (dd.mm. yy	Polarization	Pass direction
1	S1A	IW _SLC	Reference	---	----	29/1/2022	VV + VH	Ascending
	S1A	IW _SLC	secondary	24	160	22/2/2022	VV + VH	Ascending
2	S1A	IW _SLC	Reference	---	----	11/7/2023	VV + VH	Ascending
	S1A	IW _SLC	secondary	12	230	29/6/2023	VV + VH	Ascending

*Temporal baseline (Btemp), Perpendicular base line (Pperp).

4. Processing

4.1. Interferogram Formation and Coherence Estimation

An interferogram is generated by multiplying the reference image with the conjugate of the secondary image. While the phase shows the difference in phase between the two images, the amplitude of both images is multiplied. The phase difference $\Delta\varphi$ was calculated using Eq.1, these components collectively contribute to the total phase difference analysed to understand changes and topography on the Earth's surface [14], interferogram flattening (Eq. 2) was used to identify and remove the flat earth effect. Table 2 summarize all the selected parameters for interferometry processing.

$$\Delta\varphi=\Delta\varphi\text{flat}+\Delta\varphi\text{elevation}+\Delta\varphi\text{displacement}+\Delta\varphi\text{atmosphere}+\Delta\varphi\text{noise} \quad (1)$$

Where $\Delta\varphi$: is the total phase difference between the SAR images.

$\Delta\varphi$flat: The phase contribution due to the flat Earth effect.

$\Delta\varphi$elevation: The phase contribution due to topography (elevation).

$\Delta\varphi$displacement: The phase contribution due to ground displacement

$\Delta\varphi$atmosphere: The phase contribution due to atmospheric changes between times of SAR acquisitions (such as variations in humidity or atmospheric pressure).

$\Delta\varphi$noise: The phase contribution due to noise or random errors in the data.

$$\Delta\varphi_{\text{flat}} = -\frac{4\pi}{\lambda}\frac{B_n S}{R\tan\theta} \quad (2)$$

Where: B_n is the baseline component perpendicular to the line of sight

S the horizontal displacement between the reference point and the target point

λ the wavelength of the radar signal

R (line-of-sight distance) range or distance from the radar to the target

θ incidence angle which is the angle between the radar line of sight and the normal to the surface.

One helpful way to assess an interferogram quality is to look at its coherence, distinct raster called coherence is created, ranging from 0 to 1, representing the degree of pixel similarity between the two images [15].

4.2. TOPS Debursting

Bursts are temporally overlapping; debursting involves merging these overlapping bursts into a continuous image. To remove seam lines between the bursts ,Terrain Observation with Progressive Scans deburst is applied [16], TOPS deburst operator S-1 (under Radar >Sentinel-1 TOPS) is applied to the interferogram product.

4.3. Phase Filtering and Multilooking.

The interferometric phase may be affected by noise, which can reduce the quality of the interferogram. Enhancing its quality involves using an adaptive filtering algorithm that responds to local phase noise and fringe rates—such as the Goldstein filter. To apply this, the interferogram is divided into overlapping rectangular sections, and the power spectrum (u,v) for each section is calculated by smoothing the intensity of the two-dimensional Fast Fourier Transform (FFT). The filter response $H(u,v)$ is then derived from the power spectrum (Eq.4) [4]. For optimal phase unwrapping results, multi-looking is recommended. Additionally, multi-looking can be used to define a new pixel size for the image [17].

$$Z(u,v) = exp\left\{-\frac{\frac{u^2}{\sigma_u^2}-\frac{2uv}{\sigma_u\sigma_v}+\frac{u^2}{\sigma_v^2}}{2(1-\rho^2)}\right\} \quad (3)$$

$$(u,v)=|\,(u,v)\,|^{\alpha} \quad (4)$$

where α is the versatile channel boundary, u and v are the recurrence variables, $Z(u, v)$ is the Fourier range, $\sigma u2$ & $\sigma v2$ are the effective bandwidths, and ρ is the inclination range.

Table 2: Selected parameters for interferometry processing in Snap

Processing step	Parameter	Preferred value
Co-registration	Sub-swath	IW-2
	Polarization	VV
	Bursts	(5,6)
	Orbit state vectors	Sentinel precise
	Digital elevation model	SRTM 1sec HGT (auto download)
	DEM resampling method	Bilinear interpolation
Interferogram formation	Degree of Flat-Earth polynomial	5
	Number of 'Flat-Earth'	501
	Include coherence estimation	Applied
	Orbit interpolation degree	3
	Square pixel	Applied
TOPS de-burst	Polarization	vv
Goldstein phase filtering	Adaptive filter exponent in (0,1]	1
	FFT size 64	64
	Window size	3
	Use coherence mask	No Applied
	Coherence threshold in [0,1]	0.2
Phase to elevation	Digital elevation model	SRTM 1secHGT (auto download)
	DEM resampling method	Bilinear interpolation
Range Doppler terrain correction	Digital elevation model	SRTM 1arcsec
	Image resampling	Bilinear Interpolation
	Pixel spacing (m)	14.65
	Map projection	WGS84(DD)

4.4. Phase Unwrapping (Ph.U)

the phase must first be unwrapped to connect the interferometric phase to the topographic height. One of the challenges in using radar interferometry is phase unwrap, an issue brought on by the nonlinear phase structure of the system. However, there are several suggested methods for addressing the specific issue [17]. The statistical cost and network-flow methods for phase unwrapping are implemented by Snaphu, a frequently chosen unwrap program that was suggested by [18]. Numerous studies have employed Snaphu software for unwrapping procedures[19] .The altitude difference that causes an interferometric phase shift of a signal is known as the altitude of ambiguity. This uncertainty is eliminated by phase unwrapping, which integrates the phase difference between adjacent pixels [12]. Measurement of the real altitude variation is provided by the phase difference between two spots on the flattened interferogram. The wrapped phase's integer number of cycles, n, is recovered by phase unwrapping. Consequently, it is possible to ultimately determine the clear phase value ψ for every pixel Eq (5).

$$\Psi = \varphi + 2\,\pi\,n \tag{5}$$

4.5. Phase to Elevation and Terrain Correction (TC)

Unwrapped phase still not in a metric form. To convert the radian to meter unit, the phase-to-elevation operator should be applied to convert the radian units into absolute heights. It will translate the phase into surface heights. The Range-Doppler Terrain Correction (TC) will geocode

the final bands by correcting geometric distortions of SAR images by employing the SRTM 1sec digital elevation model to correct SAR geometric errors. Terrain Correction will geocode the image terrain and provide a map project.

5. Validation and Comparison

5.1.Conversion into Orthometric Height

Seintenl1-A data are ellipsoidal height provided by DLR[20]. Thus, according to [21], orthometric heights should be created. Equation (6) was used to deduct the geoid height (geoid undulation) in the EGM 96 vertical datum from the ellipsoidal Seintenl1-A heights in order to get the orthometric heights for Seintenl1-A DEM. EGM 96 could be found and downloaded from the National Geospatial-Intelligence Agency (NGA) official website (https://earthinfo.nga.mil/GandG/update/index.php?action=home).

$$H = h - N \tag{6}$$

Where (N) is the geoid height, (h) ellipsoidal height, and (H) is the orthometric height.

5.2. Statistical Assessment

In general, evaluating the quality of information collected from remotely sensed data depends on the accuracy evaluation. The vertical accuracy of the DEMs produced from Sentinel-1A in both cases was assessed, followed by the calculation of height differences between references DEM generated Fig 3 by the RTK survey points were imported into global mapper program X (Easting), Y (Northing), and Z (elevation) values in the form of a CSV format with appropriate column headers and coordinate references UTM Zone 36N (WGS 84). A gridded surface (DEM) was generated using the “Create Elevation Grid from 3D Vector Data” tool. Sentinel-1A-generated DEM Fig .4(a,b) was exported to layer new file XYZ Grid format file, each pixel has value XYZ. Add XYZ grid file on GNSS DEM surface, by analysis measurement tool, apply elevation to select feature and replace the elevation value from GNSS DEM surface and export as CSV file format.

The outlier test using interquartile range (IQR) was done based on Equation 7[22] .

$$\text{Outlier} = (Q3 - Q1) + 1.5\ \text{I QR} \tag{7}$$

Where, IQR is Interquartile range, Q1 represents the lower quartile, and Q3 is the upper quartile. Then, calculate the Root Mean Square Error (RMSE) using Equation 8 [23] .

$$\text{RMSE} = \sqrt{\frac{1}{n}\sum_{i=1}^{n}(y_i - \hat{y}_i)^2} \tag{8}$$

Where y_i it the elevation in position i of the DEM reference and $\hat{y}_i$ it the elevation for position i of the product.

5.3 Interferogram Coherence Statistics

Coherence is a measure of signal similarity between two SAR images. It ranges from 0 (no similarity) to 1 (perfect similarity). At the interferogram formation, a coherence raster is created.

Using the analysis statistics tool in the SNAP software, the statistical values for the coherence raster are calculated For model (b) (230 m Perpendicular Baseline, 12-Day Temporal Baseline) was resulted to min value = 9.4894E-4, Max =0.9536, Mean =0.5975, Median=0.6306 and Coefficient variation= 0.4884. Model (a), (160m Perpendicular Baseline, 24-Day Temporal Baseline) coherence raster was resulted to min value = 0.0013, Max =0.9534, Mean =0.4635, Median=0.4774 and Coefficient variation= 0.4612.Comparisons of the coherence statistics for Two DEMs Model (a), (b) are presented in Table 3 and showed Fig.5(a,b) .

Table 3 : Comparisons of the coherence statistics for Two DEMs Model (a), (b)

Metric	**230m, 12-Day Baseline**	**160m, 24-Day Baseline**
Mean Coherence	0.6010	0.4582
Median Coherence	0.6351	0.4705
Standard Deviation (σ)	0.1759	0.1910
Coefficient of Variation (CV)	0.4868	0.4168
ENL	4.2205	2.0193

6. Results

According to the Eldabha study area, two cross-sections were generated to assess the accuracy of the results (Fig. 2-a). The Digital Elevation Models (DEMs) derived from Sentinel-1A data after applying the Goldstein filter demonstrate significantly enhanced accuracy compared to those obtained without the filtering technique. Fig.6.(a,.b) Shows the vertical differences between the two DEMs.A statistical analysis reveals that the DEM with a shorter temporal baseline (12 days) and a larger perpendicular baseline (230 m) yielded the best vertical accuracy after applying the Goldstein filter. This DEM achieved a Root Mean Square Error (RMSE) of 12.00 meters and a Standard Deviation (STD) of 12.00 meters, indicating a higher precision in terrain representation. In contrast, the DEM with a longer temporal baseline (24 days) and a smaller perpendicular baseline (160 m), though improved by the Goldstein filter, exhibited a higher RMSE of 16.52 meters and an STD of 15.88 meters.
Before filtering, both DEMs showed considerable errors, with the DEM from the 24-day baseline configuration having an RMSE of 35.10 meters and an STD of 35.02 meters, while the 12-day baseline configuration demonstrated a slightly lower RMSE of 33.70 meters but a significantly smaller STD of 15.60 meters. These results highlight the critical role of both baseline configurations and noise filtering in determining DEM accuracy. The shorter temporal baseline and larger perpendicular baseline, coupled with the Goldstein filter, result in a more reliable and accurate representation of terrain elevation, as summarized in Table 4.

Table 4: Summary of Seintenle1-A DEMs comparison results to (GNSS)

Elevation differences	**B_{temp}/(P_{per}p)**	**Min (m)**	**Max (m)**	**Mean (m)**	**STD (m)**	**RMSE (m)**
(Before_GF) - (GNSS)	24 day 160 m	-255	203	-2.36	35.02	35.10
(After_ GF) - (GNSS)		-80.66	148	4.57	15.88	16.52
(Before_ GF) - (GNSS)	12 day 230 m	-71	22	-29.88	15.60	33.70
(After_ GF) - (GNSS)		-52	49	-2.5	12.00	12.00

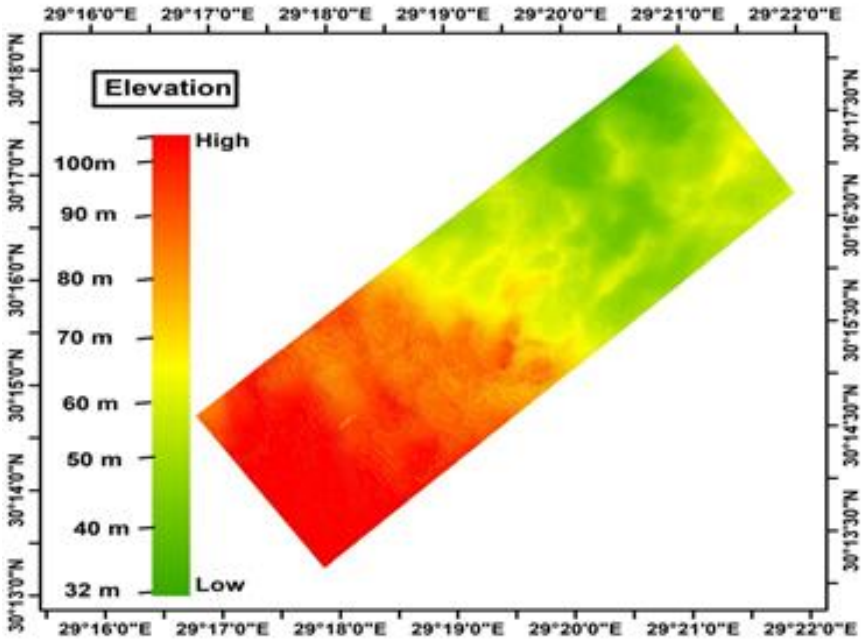

Fig.3. Reference DEM Produced from GNSS points

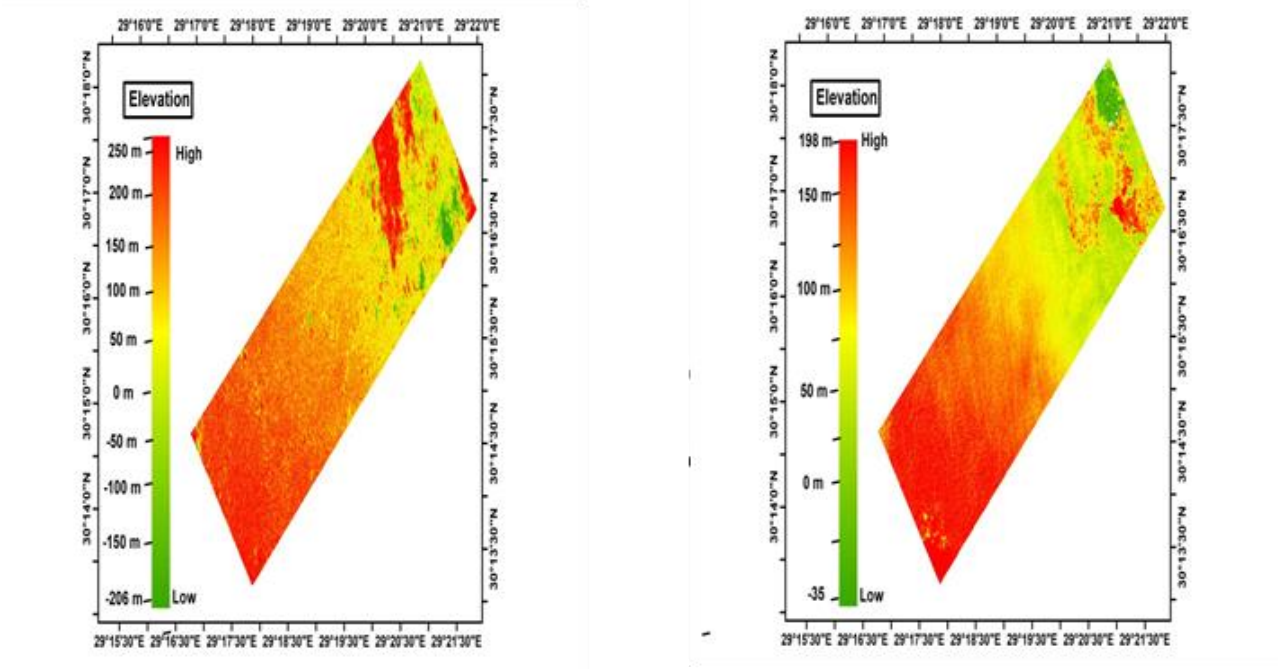

Before Goldstein Filter After Goldstein Filter

Fig 4.a Model (a) DEM extracted from Sentinel-1A

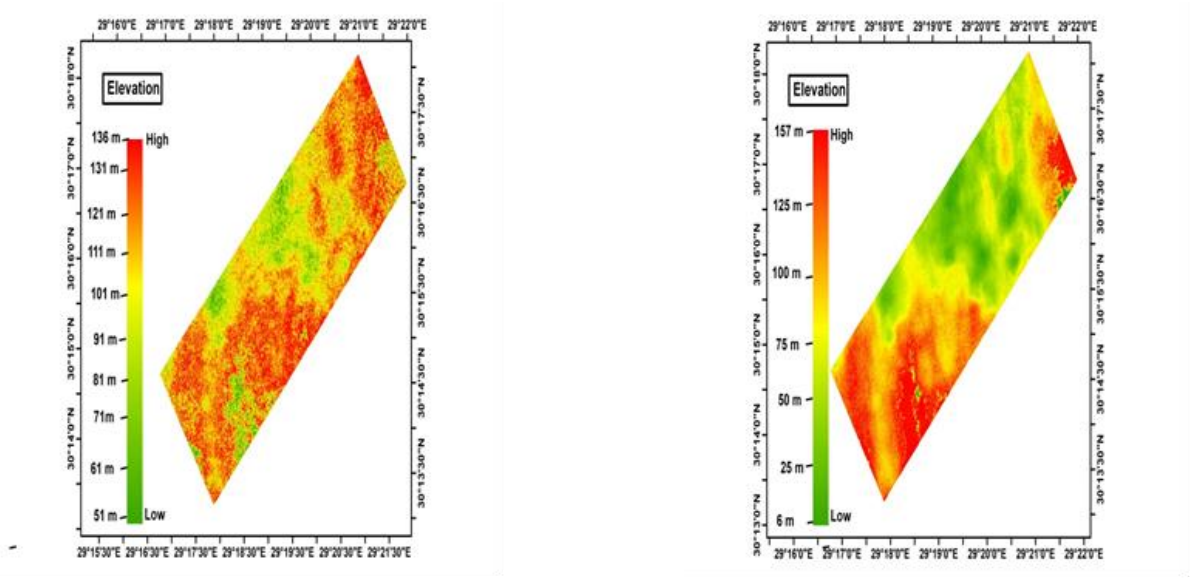

Before Goldstein Filter After Goldstein Filter

Fig4 .b Model (b) DEM extracted from Sentinel-1A

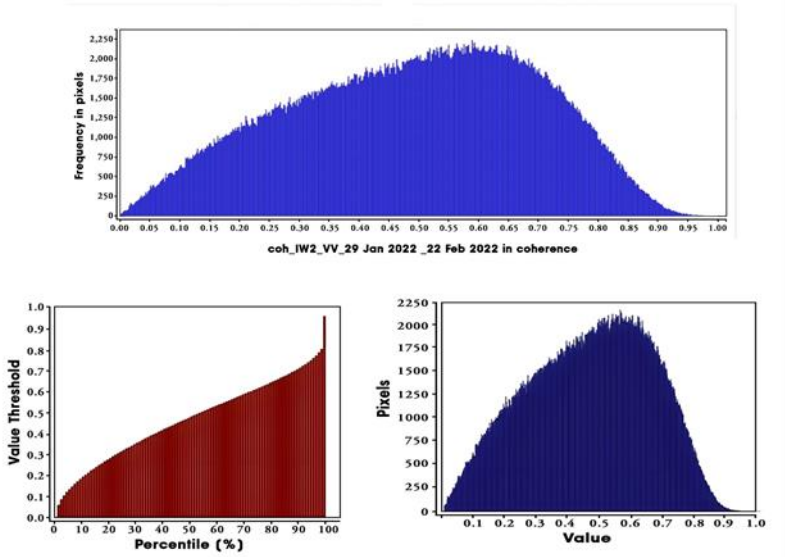

Fig 5.a Histogram & Coherence Statistics Model (a)

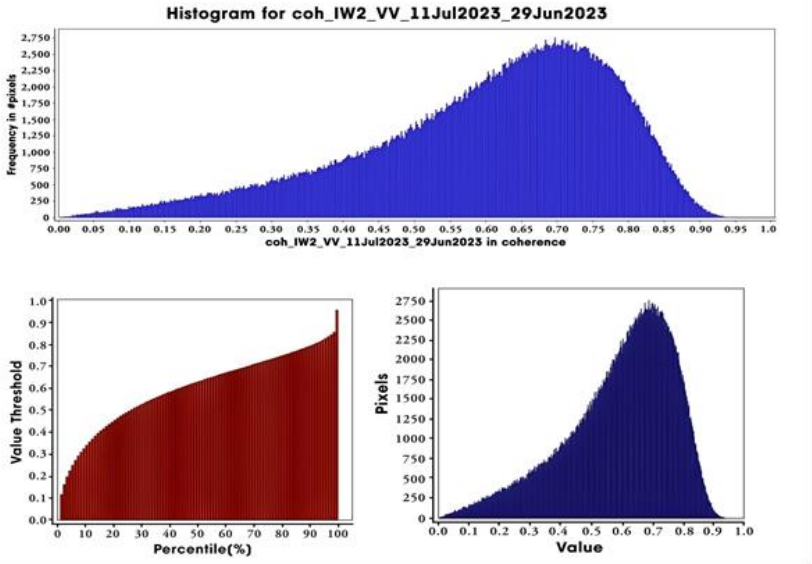

Fig 5.b Histogram & Coherence Statistics Model (b)

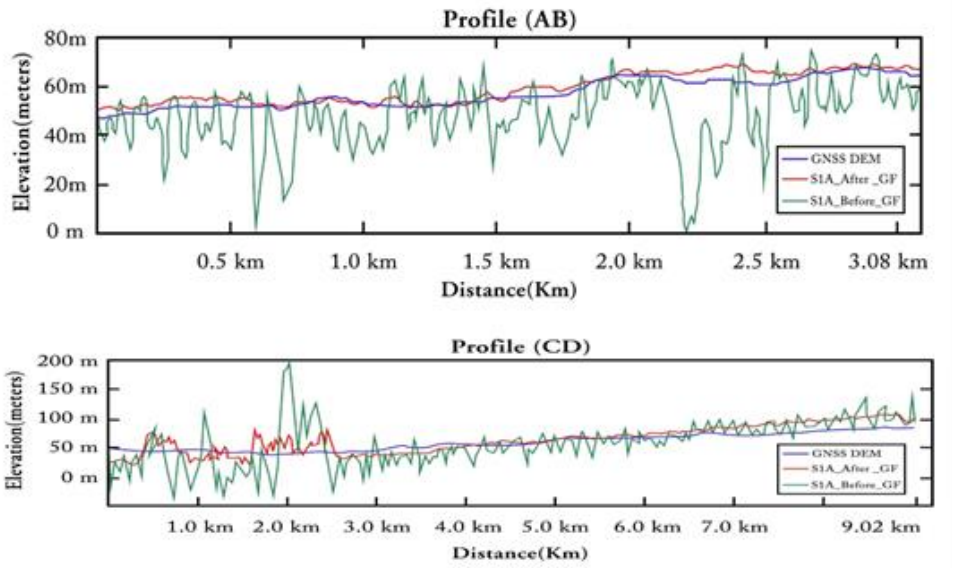

Fig.6. a The vertical differences Model (a)

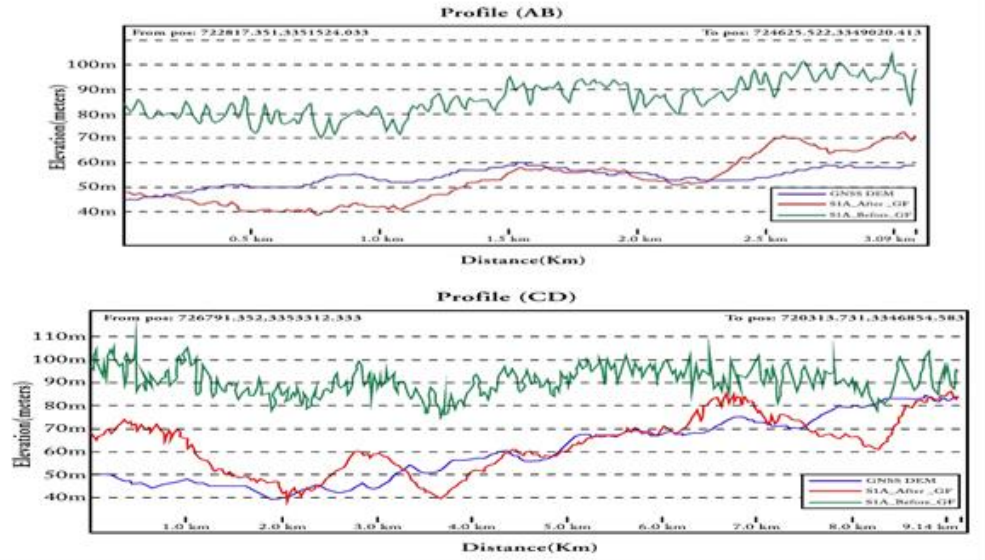

Fig.6. b The vertical differences Model (b)

7. Discussion/Conclusions

This study evaluated the vertical accuracy of DEMs derived from Sentinel-1A imagery using the InSAR technique, with a particular focus on the impact of baseline configurations and the application of the Goldstein phase filter. Two interferometric pairs were analyzed: Model (a) with a 24-day temporal baseline and 160 m perpendicular baseline, and Model (b) with a 12-day temporal baseline and 230 m perpendicular baseline. DEMs were generated under two scenarios with and without the Goldstein filter and compared against a high-accuracy GNSS-derived DEM, for a specific region of Eldabhaa .

Results showed that applying the Goldstein filter significantly enhanced DEM accuracy. For Model (a), the RMSE decreased from 35.10 m to 16.52 m, and the standard deviation improved from 35.02 m to 15.88 m, indicating better consistency and reduced noise. Similarly, in Model (b), the RMSE dropped from 33.70 m to 12.00 m after filtering, though the mean elevation error (-2.5 m) remained higher than that of Model (a), suggesting less alignment with the GNSS reference.While Model (b) benefited from a larger perpendicular baseline generally associated with improved sensitivity to

elevation differences it may have suffered from reduced coherence due to geometric decorrelation. Conversely, Model (a) demonstrated superior performance after filtering, likely due to better temporal coherence despite the longer temporal baseline. Analysis statistics for coherence Model(a) was resulted to min value = 0.0013, Max =0.9534, Mean =0.4582, Median=0.4774 and Coefficient variation =0.4162.

These findings highlight that both baseline configuration and phase filtering play crucial roles in determining DEM quality. The Goldstein filter effectively mitigates phase noise and enhances vertical accuracy, particularly when coherence is maintained. .Overall, the integration of filtering techniques and appropriate baseline selection significantly improves the reliability of InSAR-derived DEMs for geospatial applications..

References

[1] A. Braun, "Retrieval of digital elevation models from Sentinel-1 radar data - Open applications, techniques, and limitations," *Open Geosci.*, vol. 13, no. 1, pp. 532–569, 2021, doi: 10.1515/geo-2020-0246.

[2] RAMON F. HANSSEN, *RADAR INTERFEROMETRY Data Interpretation and Error Analysis*. New York, Boston, Dordrecht, London, Moscow: KLUWER ACADEMIC PUBLISHERS, 2002. doi: doi:10.1007/0-306-47633-9.

[3] P. A. Rosen, "Synthetic aperture radar interferometry," *Proc. IEEE*, vol. 88, no. 3, pp. 333–380, 2000, doi: 10.1109/5.838084.

[4] R. M. Goldstein and C. L. Werner, "Radar interferogram filtering for geophysical applications," *Geophys. Res. Lett.*, vol. 25, no. 21, pp. 4035–4038, 1998, doi: 10.1029/1998GL900033.

[5] A. Mohammadi *et al.*, "A multi-sensor comparative analysis on the suitability of generated dem from sentinel-1 sar interferometry using statistical and hydrological models," *Sensors (Switzerland)*, vol. 20, no. 24, pp. 1–24, 2020, doi: 10.3390/s20247214.

[6] K. Nikolakopoulos, A. Kyriou, and V. Charalampopoulou, "DSM generation from Sentinel and COSMO-SkyMed data using interferometry and radargrammetry: a case study from Mykonos, Greece," *Third Int. Conf. Remote Sens. Geoinf. Environ.*, vol. 9535, p. 95350H, 2015, doi: 10.1117/12.2193977.

[7] A. Mohammadi, S. Karimzadeh, and S. J. Jalal, "A Multi-Sensor Comparative Analysis on the Suitability of Generated DEM from Sentinel-1 SAR Interferometry Using Statistical and," pp. 1–24, 2020.

[8] H. Karabörk, H. B. Makineci, O. Orhan, and P. Karakus, "Accuracy Assessment of DEMs Derived from Multiple SAR Data Using the InSAR Technique," *Arab. J. Sci. Eng.*, vol. 46, no. 6, pp. 5755–5765, 2021, doi: 10.1007/s13369-020-05128-8.

[9] J. Tomaštík, J. Chudá, D. Tunák, F. Chudý, and M. Kardoš, "Advances in smartphone positioning in forests: Dual-frequency receivers and raw GNSS data," *Forestry*, vol. 94, no. 2, pp. 292–310, 2021, doi: 10.1093/forestry/cpaa032.

[10] D. Geudtner, R. Torres, P. Snoeij, M. Davidson, and B. Rommen, "'Sentinel-1 System capabilities and applications,' 2014 IEEE Geoscience and Remote Sensing Symposium," *2014 IEEE Geosci. Remote Sens. Symp.*, pp. 1457–1460, 2014.

[11] Z. Li and J. Bethel, "Image coregistration in SAR interferometry," *Proc. Int. Arch. Photogramm., Remote Sens. Spat. Inf. ...*, vol. XXXVII, no. B1, pp. 433–438, 2008, [Online]. Available: http://www.isprs.org/proceedings/XXXVII/congress/1_pdf/72.pdf

[12] F. Kervyn, "Modelling topography with SAR interferometry: Illustrations of a favourable and less favourable environment," *Comput. Geosci.*, vol. 27, no. 9, pp. 1039–1050, 2001, doi: 10.1016/S0098-3004(00)00158-8.

[13] A. Braun, "Sentinel-1 Toolbox TOPS Interferometry Tutorial," no. June, pp. 1–25, 2021.

[14] L. Braun, A., Veci, "Sentinel-1 Toolbox TOPS Interferometry Tutorial," *ESA, SkyWatch Sp. Appl. Inc*, no. June, pp. 1–25, 2021, [Online]. Available: https://skywatch.co

[15] A. Ferreti, A. Monti-Guarnieri, C. Prati, and F. Rocca, *Guidelines for SAR Interferometry Processing and Interpretation*, vol. 81, no. 17 I. 2007.

[16] N. Yague-Martinez *et al.*, "Interferometric Processing of Sentinel-1 TOPS Data," *IEEE Trans. Geosci. Remote Sens.*, vol. 54, no. 4, pp. 2220–2234, 2016, doi: 10.1109/TGRS.2015.2497902.

[17] R. L. Franceschetti, GiorgioGiorgio Franceschetti, Riccardo Lanari, Giorgio Franceschetti, *Synthetic Aperture Radar Processing /*. 2018. [Online]. Available: https://doi.org/10.1201/9780203737484

[18] C. W. Chen and H. A. Zebker, "Network approaches to two-dimensional phase unwrapping:

intractability and two new algorithms: erratum," *J. Opt. Soc. Am. A*, vol. 18, no. 5, p. 1192, 2001, doi: 10.1364/josaa.18.001192.

[19] K. Eldhuset, "Combination of stereo sar and insar for dem generation using tandem-x spotlight data," *Int. J. Remote Sens.*, vol. 38, no. 15, pp. 4362–4378, 2017, doi: 10.1080/01431161.2017.1320452.

[20] M. F. A. Rahman *et al.*, "Accuracy assessment of open-source global digital elevation models (GDEMs) with global navigation satellite system (GNSS) levelling," *IOP Conf. Ser. Earth Environ. Sci.*, vol. 1064, no. 1, 2022, doi: 10.1088/1755-1315/1064/1/012018.

[21] R. González-moradas and W. Viveen, "Remote Sensing of Environment Evaluation of ASTER GDEM2 , SRTMv3 . 0 , ALOS AW3D30 and TanDEM-X DEMs for the Peruvian Andes against highly accurate GNSS ground control points and geomorphological-hydrological metrics," *Remote Sens. Environ.*, vol. 237, no. April 2019, p. 111509, 2020, doi: 10.1016/j.rse.2019.111509.

[22] P. J. Rousseeuw and M. Hubert, "Robust statistics for outlier detection," vol. 1, no. February, pp. 73–79, 2011, doi: 10.1002/widm.2.

[23] C. Res, C. J. Willmott, and K. Matsuura, "Advantages of the mean absolute error (MAE) over the root mean square error (RMSE) in assessing average model performance," vol. 30, pp. 79–82, 2005.

[24] H. A. Zebker and J. Villasenor, "Decorrelation in interferometric radar echoes," *IEEE Trans. Geosci. Remote Sens.*, vol. 30, no. 5, pp. 950–959, 1992, doi: 10.1109/36.175330.

[25] H. a Zebker and P. a Rosen, "Atmospheric Artifacts in Interferometric SAR Surface Deformation and Topographic Maps," *J. Geophys. Res.*, vol. 99, no. 19, pp. 617–634, 1996.